THE JOURNAL OF COMPARATIVE NEUROLOGY 409:573–591 (1999)

Relationships Between Cytochrome Oxidase (CO) Blobs in Primate Primary Visual Cortex (V1) and the Distribution of Neurons Projecting to the Middle Temporal Area (MT)

JAMIE D. BOYD[1] **AND VIVIEN A. CASAGRANDE**[1,2,3]*
[1]Department of Cell Biology, Vanderbilt University, Nashville, Tennessee 37232
[2]Department of Psychology, Vanderbilt University, Nashville, Tennessee 37232
[3]Ophthalmology and Visual Sciences, Vanderbilt University, Nashville, Tennessee 37232

ABSTRACT

The cytochrome oxidase (CO) blobs and interblobs in layer 3B of primate visual cortex have different sets of corticocortical connections. Cortical layers below layer 3B also project corticocortically, but the relationship of efferent projections from the deeper layers to the overlying blob/interblob architecture is less clear. We studied the tangential organization of neurons projecting from primary visual cortex (V1) to the middle temporal visual area (MT) and their relationship to the CO blobs. MT-projecting neurons in two primate species, bush babies and owl monkeys, were retrogradely labeled, then charted in tangential sections, and compared to the positions of the overlying CO blobs. In both primate species, MT-projecting neurons in layer 3C were unevenly distributed in the tangential plane, with dense patches of labeled cells that were aligned with the CO blobs. A novel two-dimensional spatial correlation method was used to show the colocalization of MT-projecting cells with the overlying blobs. Chi-square analyses performed with the cortical surface equally divided into compartments of blob, interblob, and blob/interblob borders showed that blob columns tended to have about 1.5 times more MT-projecting cells ($P < 0.0001$) than interblob columns. Similar analyses were applied to published data on V1 cells projecting to area MT in macaque monkey (Shipp and Zeki [1989] Euro J Neurosci 1:310–332). Again, the results showed a significant correlation between the cell distribution and CO blobs. Taken together, these results suggest that layer 3C is not uniform but is made up of a mosaic of cells that project to area MT and cells that project to some other location. These findings also indicate that the mosaic organization of layer 3C is related in some unique way to the overlying CO architecture. J. Comp. Neurol. 409:573–591, 1999.

Indexing terms: owl monkey; bush baby; striate cortex; parallel pathways

Patchy, periodic clustering of projection cells has long been known to characterize the efferent pathways from layer 3 of the primary visual cortex to extrastriate areas in primates (Wong-Riley, 1979b). This clustering has been shown to correspond to a regular array of patches, or blobs, revealed by staining for the metabolic enzyme cytochrome oxidase (CO) in a number of primate species, including macaque monkey (Horton and Hubel, 1981), owl monkey (Tootell et al., 1985), and bush baby (Condo and Casagrande, 1990). (For reviews, see DeYoe and Van Essen, 1988; Martin, 1988; Wong-Riley, 1989, 1994). For example, cells in the densely staining blobs make connections with a different set of compartments (also defined by CO staining) in the secondary visual cortex (V2) than do the lightly staining interblobs; a small injection confined to

Grant sponsor: NIH; Grant number: E401778; Grant number: EYO8126; Grant number: HD15051.

All of the Igor Pro 3.1 procedure files that were written for this study are freely available for downloading at 160.129.89.116/jamie.html.

*Correspondence to: Vivien A. Casagrande, Department of Cell Biology, Vanderbilt University Medical School, MCN C2310, 1161 21st Avenue South, Nashville, TN 37232–2175.
E-mail: Vivien.Casagrande@mcmail.Vanderbilt.edu

Received 31 August 1998; Revised 5 January 1999; Accepted 11 February 1999

a single compartment in V2 will label either blobs or interblobs, but not both, giving rise to a patchy pattern of labeling in V1 (Livingstone and Hubel, 1983, 1984). Also, certain areas may receive projections specifically from one or the other compartments. The connections of the Dorsal Medial Area (DM) defined in New World primates and bush babies (Lin et al., 1982; Krubitzer and Kaas, 1993; Rosa and Schmid, 1995) also show a relationship to the CO architecture of V1 (Krubitzer and Kaas, 1990, 1993; Beck and Kaas, 1998a,b).

The blobs are most visible in layer 3B, where they have been shown to correspond to patches of geniculate input in bush babies (Lachica and Casagrande, 1992), New World monkeys (Fitzpatrick et al., 1983; Diamond et al., 1985; Ding and Casagrande, 1997), and Old World macaque monkeys (Livingstone and Hubel, 1982; Hendry and Yoshioka, 1994). However, more subtle differences in CO staining between blobs and interblobs can be seen in other cortical layers (Horton and Hubel, 1981; Hendrickson, 1985; Tootell et al., 1985; Condo and Casagrande, 1990) (In this article, we refer to the patches of dense CO staining in layer 3B as the CO blobs proper, and refer to an entire column of cortex containing a blob as a CO blob column.) In addition, differences in the intrinsic vertical connections within cortex have been demonstrated between blobs or interblobs in layer 3B (Lachica et al., 1992, 1993; Yoshioka et al., 1994). Thus, distinctions between blobs and interblobs might be expected to be present throughout the cortical column. In fact, reports of connectional differences between blob and interblob columns have also been seen in the infragranular layers; there is a lower density of Meynert cells (Fries, 1986; Payne and Peters, 1989) and corticocollicular cells in general (Lia and Olavarria, 1996) under CO blobs.

In this paper, we examine the distribution of another class of projection cells: those projecting to the middle temporal visual area (MT). MT is an extrastriate area generally agreed to be concerned with motion processing (Zeki, 1974; Albright, 1984; Boussaoud et al., 1990; Felleman and Kaas, 1984; Albright, 1992). The cells projecting from V1 to MT are found in layers 3C and 6. Layer 3C of Hässler (1967), equivalent to Brodmann's (1909) layer 4B (for review of lamination issues, see Casagrande and Kaas, 1994), is below layer 3B, the layer containing the CO blobs. MT-projecting cells in layer 3C are located directly above 4α, the input zone of the magnocellular geniculate layers (Tigges et al., 1981; Diamond et al., 1985; Shipp and Zeki, 1989), and inactivation of the magnocellular or parvocellular geniculate layers shows that responses in MT are dependent mainly on magnocellular, not parvocellular, inputs channeled through V1 (Maunsell et al., 1990). Layer 3C contains a high proportion of directionally selective cells (Blasdel and Fitzpatrick, 1984; DeBruyn et al., 1993), and a recent study using antidromic activation has confirmed that the V1 neurons projecting to MT are direction-selective (Movshon and Newsome, 1996). Thus, a relationship between MT-projecting cells and CO blob/interblob columns might suggest a tangential segregation within V1 of a particular class of input coming from the magnocellular layers of the LGN via V1 and terminating in MT.

Only one previous study has examined the relationship between MT-projecting cells and CO compartments (Shipp and Zeki, 1989). This study found that, in macaque monkeys, MT-projecting cells in V1 were not evenly distributed tangentially, but were clustered. However, this study found no consistent relationship between these clusters of MT-projecting cells and overlying CO blobs in V1. The authors concluded that some other tangential organizing principle, with a similar periodicity to, but distinct from, the CO blobs, was responsible for the clustering of the MT-projecting cells.

Neurons projecting to MT in owl monkeys and bush babies were retrogradely labeled and compared to the overlying pattern of CO staining. In these primates, a clear relationship was found between CO staining in layer 3B and MT-projecting neurons in layer 3C: MT-projecting neurons in both species were more numerous below CO blobs than below interblobs, suggesting that functional compartments related to blob/interblob distinctions also exist in layer 3C. An abstract of some of these findings has been previously published (Boyd and Casagrande, 1996).

METHODS AND MATERIALS

Experimental animals

Data presented here were obtained from three bush babies (*Otolemur garnettii*; also known as *Galago crassicaudatus garnettii*; case numbers 95–33, 96–30, and 95–32) and three owl monkeys (*Aotus trivirgatus*; case numbers 96–17, 96–38, and 96–41). Each animal received unilateral injections of the neuroanatomical tracer cholera toxin subunit B conjugated to 7 nm colloidal gold particles (CTB-Au, List Biological, Campbell, CA; 1% in 0.9% sterile saline) into the middle temporal (MT) area. All animals were cared for according to the National Institutes of Health Guide for the Care and Use of Laboratory Animals and the guidelines of the Vanderbilt University Animal Care Committee under approved protocols.

Surgical procedures: Bush babies

The anatomical experiments reported here were done in conjunction with unrelated electrophysiological experiments on the other hemisphere that necessitated an acute preparation (for details, see DeBruyn et al., 1993). Prior to being anesthetized, animals were given intramuscular injections of 0.5 mg/kg acepromazine maleate and 0.05 mg/kg atropine sulfate. Animals were also given an intramuscular injection of dexamethasone (0.2 mg/kg) to reduce brain edema.

Surgical anesthesia was induced with trifluoroethane (halothane, Halocarbon Laboratories, River Edge, NJ). A femoral vein was cannulated and anesthesia was then switched to i.v. infusion with propofol (Zeneca Pharmaceuticals, Wilmington, DE). In preparation for the acute recording session, a tracheotomy was also performed at this time, and a small craniotomy was made over the intended recording site in the other hemisphere. For the MT injections described here, the skull and dura was removed from a roughly 4 mm $\times$ 4 mm square centered on a point 13 mm lateral from the mid-sagital suture, and 13 mm anterior from the posterior pole of the cortex.

After surgery was completed, animals were paralyzed with pancuronium bromide (1.9 mg/kg/hr; Gensia laboratories, San Diego, CA) and artificially respired with a mixture of 70% nitrous oxide and 30% oxygen with 1.5% CO_2 added. End-tidal CO_2 was maintained at 4%. Animals were continuously infused with 5% dextrose in lactated Ringer's Solution and propofol (about 0.5 mg/kg/hr); adequate levels of anesthesia were maintained by continu-

ously monitoring EKG and EEG. Rectal temperature was monitored and maintained at 37.5° with a heating pad. The electrophysiological experiments ranged in length from 1 to 3 days, after which time the animal was given an overdose of barbiturate anesthetic and perfused.

Surgical procedures: Owl monkeys

Injections in owl monkeys were done as recovery surgeries, under aseptic conditions. Prior to surgery, animals were given atropine sulfate (0.1 mg/kg) and dexamethasone (0.2 mg/kg). Animals were anaesthetized with isofluorane in oxygen, intubated, and placed in a stereotaxic apparatus. Heart and respiration rates were monitored throughout the surgery, and muscle tone and corneal blink reflexes were tested periodically. Rectal temperature was monitored, and each animal was kept warm with a water-circulating heating pad.

The skull was removed from a roughly 1-cm square over the middle of the temporal lobe, and the dura was resected. Injections were made into a region immediately posterior to the dorsal tip of the superior temporal sulcus. Following completion of the injections, the dural flap was repositioned over the cortex, and the skin was sutured. Postoperatively, animals were given penicillin (flocillin, Fort Dodge Laboratories, Fort Dodge, IA; 300,000 units) and banamine (Fort Dodge Laboratories; 0.02 mg/kg), and/or torbugesic (Fort Dodge Laboratories; 0.05 mg/kg) as analgesics. After a survival period of 2 days, the animals were given an overdose of barbiturate anesthetic and perfused.

Tracer injections

Tracer was injected using glass micropipettes (inner tip diameter of 20 μm) by applying air pressure using a syringe coupled with tubing to the back of the pipette. In bush babies, 5–10 small injections were made in a matrix with a spacing of about 500 μm. In owl monkeys, more injections were made, covering about twice as much area. About 5 μl total of tracer was injected into MT of each bush baby, and about 10 μl into MT of each owl monkey.

Histology

Animals were perfused transcardially with 750 ml of phosphate buffer (0.1 M, pH 7.2) with 0.5% sodium nitrite followed by 400 ml of 2% paraformaldehyde and 0.1% glutaraldehyde in phosphate buffer. The brain was divided with a cut immediately anterior to the temporal lobe, and the posterior portion of cortex was removed from the brainstem and then manually flattened before sectioning. To relieve the intrinsic curvature of the cortical mantle, a single cut was made on the medial surface of the hemisphere through the calcarine sulcus, separating upper from lower paracentral and peripheral visual field representations of V1 at the approximate level of the horizontal meridian. The flattened cortical blocks were left overnight in 2% paraformaldehyde and 30% sucrose in phosphate buffer, equilibrated in 30% sucrose, and then sectioned tangentially at 50 μm.

CTB-Au was visualized by silver intensification using the IntenSE M kit (Amersham Life Science, Arlington Heights, IL). Equal amounts of solution A, solution B, and distilled water were mixed together, and free-floating sections were incubated with agitation and protected from direct light for times ranging from 1 to 2 hours. In some cases, additional silver in the form of silver nitrate (0.05–0.10%) was added to enhance the reaction. Sections stained for CTB-Au were counterstained for Nissl substance with Cresyl violet, or for cytochrome oxidase activity (CO) using the protocol of Wong-Riley (1979a). In order to obtain good CO staining, it was essential to do the CO staining first, followed by the silver intensification. Selected sections through the superficial layers were reacted with a nickel- and cobalt-enhanced CO stain (Boyd and Matsubara, 1996). To identify MT based on its distinctly dense myelination (Allman and Kaas, 1971; Allman et al., 1973), selected sections through the deeper cortical layers were stained for myelin with a silver stain (Gallyas, 1979).

Data analysis

Data from tangential tissue sections were encoded with the Bioquant computer analysis system (R and M Biometrics, Nashville, TN) or a system based on a Power Macintosh computer running Igor Pro 3.1 (Wavemetrics, Inc., Lake Oswego, OR). For each experiment, a region of V1 (or sometimes two regions) with dense labeling and even CO staining was marked off on each tissue section. Choosing small areas with even CO staining was necessary because fluctuations in CO staining caused by the level of the section passing through different cortical layers would interfere with our methods of assigning CO compartments (see below). The positions of all labeled cells in the marked off region were encoded, as well as the positions of many radially penetrating blood vessels, the latter being used as landmarks to align serial tangential sections. Digital images of CO-stained sections were captured with a Power Macintosh computer using Photoshop (Adobe Systems Inc., San Jose, CA) software and a Leaf Lumina digital camera (Scitex America, Bedford, MA) mounted on a Nikon (Atlanta, GA) compound microscope equipped with 0.5× and 4× lenses. When capturing images of double-labeled sections, care was taken to choose sections from just above the layer of cortex containing MT-projecting cells. In this way, the image reflected CO staining alone, and not CO staining plus the black MT-projecting cell bodies. Using routines written in Igor Pro 3.1, the x–y-coordinate data from different serial sections and the digitized CO images were aligned to each other using radially penetrating blood vessels, which were encoded along with the labeled cell data, and which were visible in the digitized images of the CO sections. Images of CO-stained sections were initially captured at high resolution, then interpolated to a constant resolution of 50 pixels/mm for analysis.

To complement the data generated from this study, data from Shipp and Zeki's (1989) study on MT-projecting cells and CO blobs in macaque monkeys was also examined. Their figures 11 and 13a were scanned at high resolution on a Epson (Torrence, CA) flat bed scanner connected to a Macintosh computer and imported into Igor Pro 3.1, where the positions of MT-projecting cells marked on the original figures were recorded. Then, the markers for labeled cells and the scale bar were erased from the CO image by filling them in with values obtained from an averaging of the area within a 50-μm radius of the marker/scalebar.

Two different methods were used to examine the relationship between CO staining and MT-projecting neurons. A χ^2 analysis was used to determine if the density of cells inside and outside of blobs was significantly different from chance. Positions of blobs and interblobs were determined by the following process. The CO image was low pass filtered with a radius of 150 μm to remove low-frequency fluctuations in

staining density not related to CO blobs, and then smoothed with a Gaussian convolution of radius 100 μm. The pixels in the image were then divided into three groups based on image value. The levels for division were chosen so that, as far as possible, the number of pixels in the high, medium, and low levels were approximately equal. In this manner, CO blobs (the areas of highest staining density) corresponded to about one-third of the cortical area, which is in approximate agreement with results based on "by eye" estimates of blob/interblob areas (Condo and Casagrande, 1990). Dividing the remaining two-thirds of the cortical area into two compartments was done in recognition of the fact that blob/interblob borders are not sharp and distinct but gradual and fuzzy. Other studies have used a similar three-way division of cortex into blob cores, blob margins, and interblobs in their analyses (Payne and Peters, 1989; Shipp and Zeki, 1989; Lia and Olavarria, 1996). Igor Pro 3.1 was programmed to count the cells in blobs and interblobs, to calculate the exact area of blobs and interblobs, and to compute the χ^2 statistic. In those cases where two analysis regions were examined, the data from the two regions were pooled when recording the densities of cells in the CO compartments.

The second analysis routine involved an adaptation of the density recovery profile of Rodieck (1991), which has previously been used to examine the relationship between retrogradely labeled cells and CO staining (Lia and Olavarria, 1996). In that study, the average density of labeled cells at different distances from CO blob centers was compared. Here, the average density of CO staining at different distances from labeled cells was calculated. With this method, if cells are concentrated in CO blobs, then CO staining density will be higher than average near labeled cells; i.e., there will be a dark spot at the origin of the plot. Moreover, the dark spot will have the same size, shape, and orientation as an average CO blob. Thus, correlations in CO staining and labeling density due to alignment with the overlying blobs/interblobs can be distinguished from any chance correlations due to periodicities different from that of the overlying CO blobs.

RESULTS

Injection sites

The purpose of this study was to examine the organization of cells projecting from the primary visual cortex (V1) to the middle temporal area (MT). Because MT is bordered by cortical areas that also receive projections from V1 (Allman and Kaas, 1974; Krubitzer and Kaas, 1986; Kaas and Morel, 1993; DeYoe et al., 1994), it was necessary to ensure that the injections of tracers were confined to MT. Fortunately, MT can be easily recognized by virtue of its dense myelination (Allman and Kaas, 1971; Allman et al., 1973). Figure 1 shows examples of the location relative to the cortical myeloarchitecture of injection sites made for these experiments. Figure 1A shows a tangential section of posterior neocortex from bush baby 95–32. Figure 1C shows a tangential section from owl monkey 96–38. Both sections have been stained for myelin. In both cases, MT can be visualized as a densely staining oval shaped area. Figures 1B and 1D show more superficial sections from the same cases as 1A and 1C, respectively. These sections have been stained for cytochrome oxidase (CO) as well as being reacted to visualize the gold conjugated cholera toxin (CTB-Au) used as a tracer. In both cases, the injection sites are confined to the myelin-dense zone known to correspond to MT. Also, it can be seen that the injection sites comprise a relatively large proportion (20–25%) of the total area of MT.

Other features of cortical architecture are also visible in these sections, most notably the border between areas V1 and V2. In the bush baby case in Figure 1A,B, the plane of section through V1 passes through the middle cortical layers, and V1 is more darkly stained for myelin than V2; while in the owl monkey case (C,D), the section is from the deeper cortical layers, below the densely myelinated stria of Gennari, and V1 appears less densely stained than V2. For the same reason, CO blobs are present in V1 of Figure 1B, but are not seen in V1 in Figure 1D, because the section passes through the bottom of layer 4, which is densely and continuously stained for CO.

Laminar organization of MT projections

The laminar organization of MT-projecting neurons found in this study was in general agreement with results reported elsewhere for both bush babies (Diamond et al., 1985) and owl monkeys (Diamond et al., 1985; Shipp and Zeki, 1989). To describe lamination in this paper, we use a modified form of the lamination scheme of Hässler (1967) in place of the more commonly used scheme of Brodmann. For the purposes of this study, it is sufficient to note that Brodmann's layer 4C is equivalent to Hässler's layer 4, and Brodmann's 4A and 4B are considered as sublayers of layer 3 in the present scheme. As reviewed in Casagrande and Kaas (1994), our modification of Hässler's scheme has the advantage that it is easier to compare lamination across species; using this scheme, MT-projecting cells are found in layer 3 in bush babies and owl monkeys, whereas in Brodmann's scheme, MT-projecting cells are in a sublayer of layer 4 in owl monkeys, and in layer 3 in bush babies.

In both bush baby (Fig. 2A,C) and owl monkey (Fig. 2B), MT-projecting neurons (black) are concentrated in the bottom of layer 3 (3C). The sections shown in Figure 2 also were counterstained with CO (brown), which is known to colocalize with areas of direct geniculate inputs—showing that the MT-projecting cells lie immediately above the main geniculate input zone in layer 4, which is CO-dense. In the owl monkey, MT-projecting cells are homogenous in size and form a narrow row, corresponding to a relatively CO-pale layer 3C. In the bush baby, there is no CO-pale layer 3C, and the CO blobs of layer 3B appear to pass through 3C, reaching the top of layer 4. This lack of sublamination is mirrored in the location of the MT-projecting cells, which, while most numerous in the deepest part of layer 3, as in owl monkeys, are scattered from layers 3A to 3C. The MT-projecting cells in bush babies are also heterogeneous with respect to cell size (Fig. 2B). In bush baby, a few MT-projecting cells are also found within layer 4α (Fig. 2C), which is never the case in the owl monkey.

In both primate species, a small number of large pyramidal cells are also labeled in the infragranular cortical layers. This subpopulation of large pyramidal cells stains strongly for CO. In the owl monkey (and other simian primates), these large CO-containing pyramidal cells are known as Meynert cells (Chan-Palay et al., 1974; Spatz, 1975; Winfield et al., 1981; Fries et al., 1985; Payne and Peters, 1989) and are found at the border between layers 5 and 6; while in the bush baby, they are found in a narrow

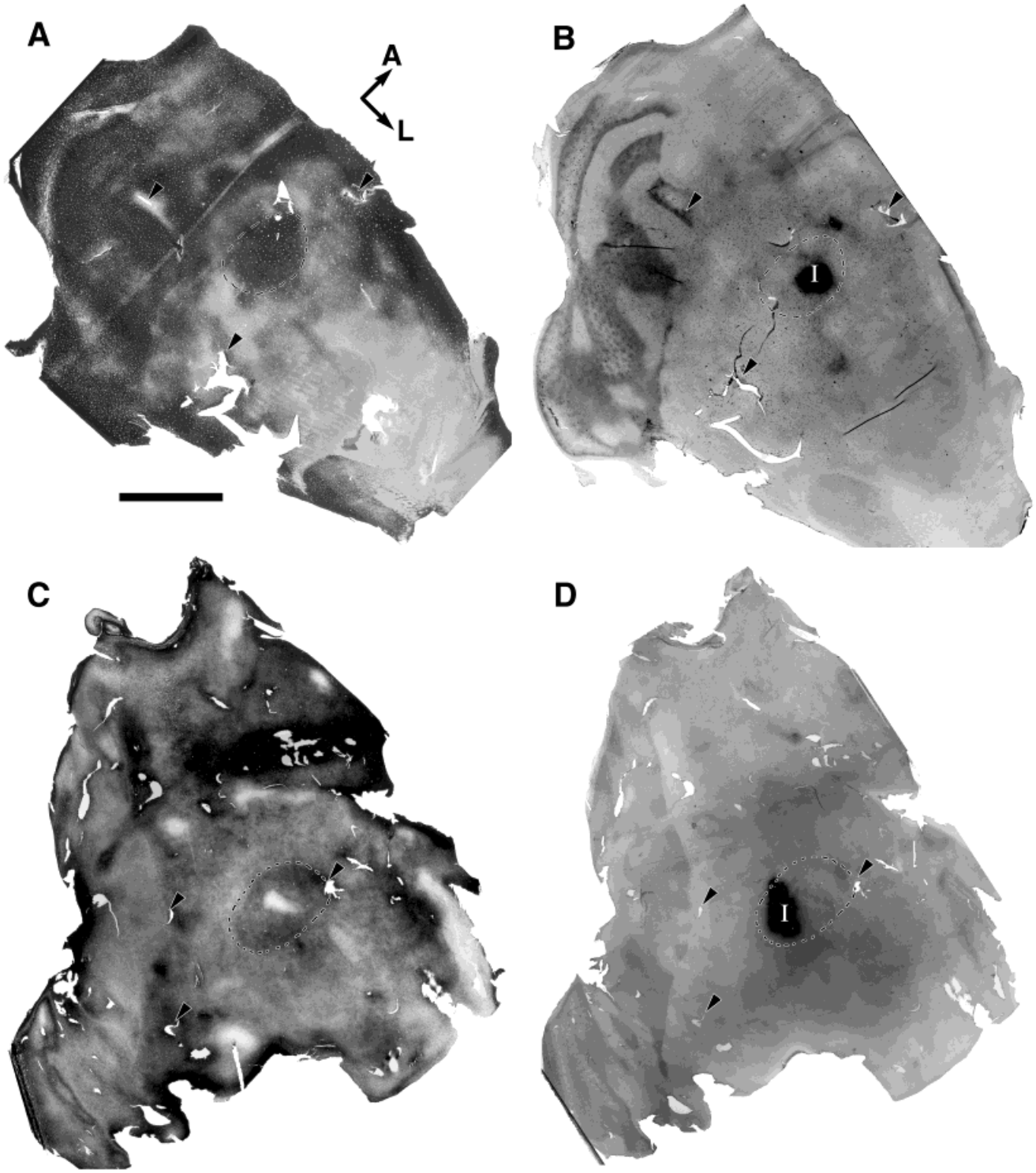

Fig. 1. Examples of middle temporal area (MT) injection sites. **A:** A tangential section from the lower cortical layers of bush baby 95-32 stained for myelin. An oval area darkly stained for myelin (outlined with a dashed line) is seen in the expected location of MT. The arrows show the anterior ("A") and lateral ("L") directions relative to the position of the cortex in the intact brain. **B:** A cytochrome oxidase (CO) stained section from the middle cortical layers of the same hemisphere seen in Figure A also reacted for CTB-Au to reveal the tracer injection site (I). The dashed oval was copied directly from A and overlaid on this section to show the position of the injection site relative to MT. Arrowheads show corresponding artifacts in the two sections. The CO staining shows the borders of the primary visual cortex (V1); where the plane of the section passes through layers 3 and 4α of V1, CO blobs are visible. **C, D:** A pair of tangential sections from owl monkey 96-38 stained for myelin and CO plus CTB-Au, respectively. The section in D passes mostly through the bottom part of layer 4, so the CO blobs of layer 3 are not seen throughout most of V1. Scale bar = 10 mm and applies to A–D.

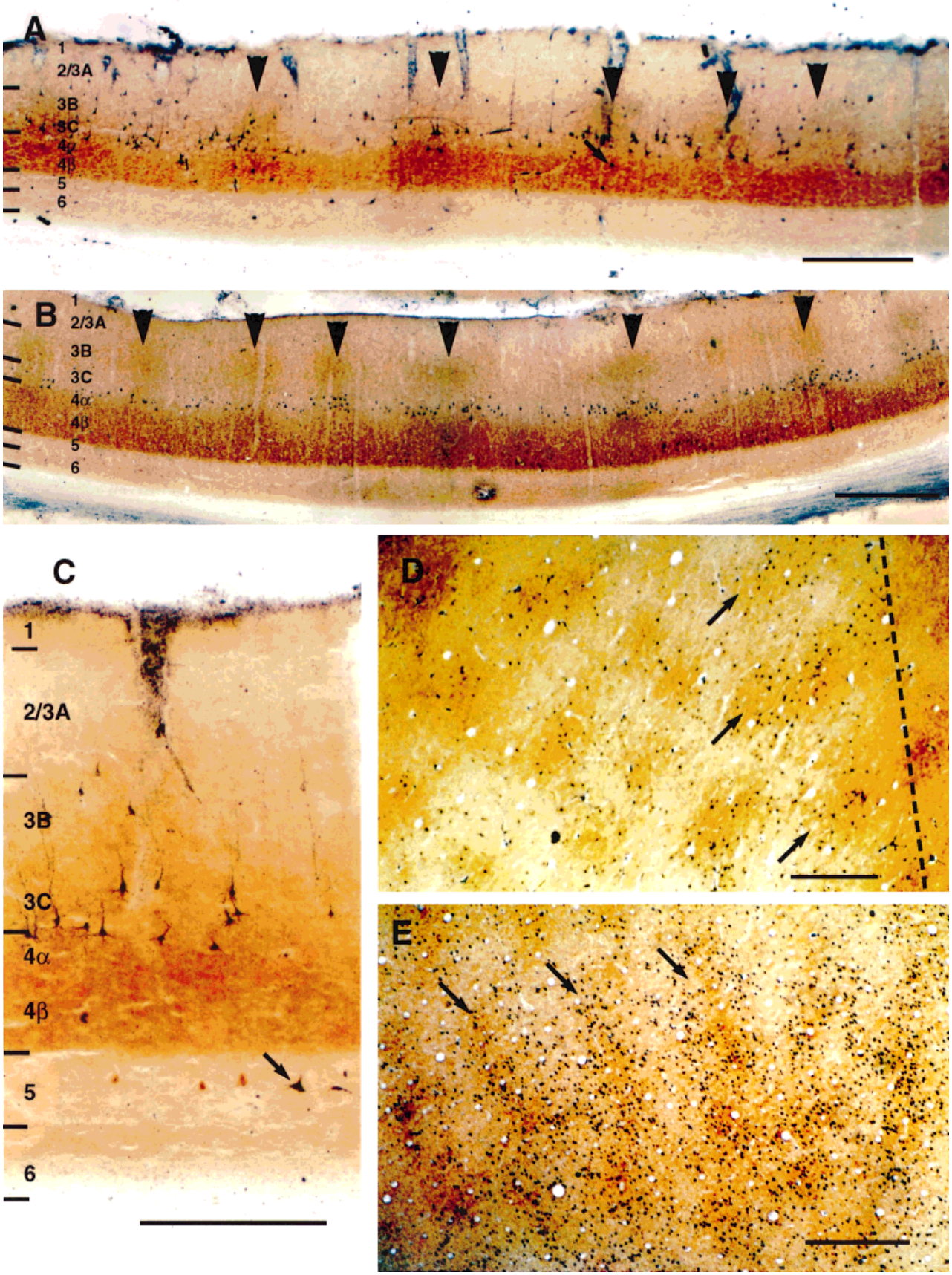

Figure 2

sublayer in the middle of layer 5 (Condo and Casagrande, 1990) and are more numerous than are Meynert cells in simian primates. Although all of the infragranularly located MT-projection cells in bush baby and owl monkey are stained for CO, only a small number of the CO-containing pyramidal cells are retrogradely labeled, even in the areas of densest labeling. In the quantitative analysis of retrograde labeling and CO staining below, infragranular cells were analyzed separately from cells in layer 3, because their distributions appeared to differ significantly.

Tangential organization of MT-projecting cells: Relationship to CO blobs

Even in the transverse sections of Figures 2A (bush baby) and 2B (owl monkey), it can be seen that MT-projecting cells are not uniformly distributed tangentially; instead, it appears that there are more cells underneath the CO blobs than underneath the interblobs. This impression is supported by Figure 2D (bush baby 95–32) and 2E (owl monkey 96–41), which show tangential sections through the lower part of layer 3 double-stained for retrogradely labeled cells (black) and CO (brown). In bush baby, the CO blob staining pattern of layer 3B extends through layer 3C to layer 4α, so a single tangential section can show both MT-projecting cells and good staining of CO blob columns. MT-projecting cells in owl monkey are found in a CO-poor sublayer (layer 3C). Nevertheless, CO dense and light distinctions can still be seen in the tangential sections through layer 3C containing the labeled cells, albeit not as clearly as in layer 3B. In both species it appears that MT-projecting cells tend to be located beneath blobs rather than interblobs. This was perhaps more clear for the bush baby than for the owl monkey; in owl monkeys a larger number of cells also are present below the interblobs.

Bush baby layer 3. The preference of MT-projecting cells for the CO blob columns versus the interblob columns was examined quantitatively in three bush baby hemispheres sectioned tangentially. Figure 3 shows the analysis for the distribution of retrogradely labeled cells in layer 3 of bush baby 95–33. The region from which labeled cells were charted included that part of V1 containing dense labeling, as well as a narrow strip of V2 adjoining V1. Labeling was also found in other cortical areas, in agreement with previous studies (Krubitzer and Kaas, 1990b). A surface view of retrogradely labeled cells composited from a series of tangential sections is shown in Figure 3A. The region shown contains the upper visual field representation of V1, with more central fields represented more medially and anteriorly. Each dot represents a single retrogradely labeled neuron; the clustering of MT-projecting cells is evident in this reconstruction. To more easily identify clusters of neurons, a Gaussian filter (see Materials and Methods) was used to generate an image of the labeling data. The image generated from applying this procedure to the boxed area "1" in Figure 3A is shown in Figure 3B. In this type of smoothed image, dense patches of labeled cells were easy to identify. The centers of some of these patches, as identified by eye, are marked by asterisks. The pattern of CO staining for this experiment is shown in Figure 3C. The CO-stained section was aligned with the sections containing retrogradely labeled cells using blood vessels as landmarks. The asterisks shown in Figure 3B were transferred to the corresponding locations on the CO-stained section, serving as visual landmarks for a "by eye" comparison of MT-projection cell density and CO staining. Nearly all of the patches of labeled cells correspond to a blob in the CO-stained section.

A three-way χ^2 analysis was performed on the data in Figure 3, dividing the cortex into three approximately equal sized compartments, blob, blob borders, and interblobs, using the procedure described in Methods. In Figure 3D, the blobs are shown outlined and the retrogradely labeled cells are superimposed on top of them. For clarity, only the outlines of blobs are shown; the remaining cortical area thus includes both interblobs and blob borders. The results from the χ^2 analysis from this experiment are shown in the first row of Table 1. In this case, there is a more than 1.5 times greater density of MT-projecting cells in the blob column than in the interblob column, with an intermediate density in the blob border column. The results are significantly different from the distributions that would be expected by chance alone.

Attempting to draw the sharp borders necessary when subdividing the cortex into CO compartments for a χ^2 analysis introduces certain problems. Therefore, the relationship between the MT-projecting cells and the CO architecture was also studied using a two-dimensional spatial cross-correlation method (see Materials and Methods) (Fig. 3E,F). Given two populations of labeled cells, Rodieck's (1991) method calculates the probability of encountering a cell of the second population at different distances from cells of the first population, showing whether the two populations tend to be segregated from each other or clustered together, and over what distance the relationship holds. Our method calculates the average intensity value of an image (in this case an image of a CO-stained section) at different distances from a population of labeled cells, showing whether the cells are associated preferentially with dark or light areas of the image, and the spatial extent of the relationship. Figure 3E shows the correlation between CO staining and MT-projecting cells for the same data shown in Figure 3B–D. The reference position, (0,0) is in the center of the figure. The darkness of the image at different x–y-distances from the reference position corre-

Fig. 2. Photomicrographs of middle temporal area (MT) projecting cells (dense black label) in sections also stained for cytochrome oxidase (CO) (lighter brown stain), showing the relationship of the MT-projecting cells to the layers and compartments defined by CO activity. **A:** Photomicrograph of a section from bush baby 96-30. This portion of the section was cut transverse to the cortical layers, which are marked. MT-projecting cells are found throughout layer 3, most commonly in layer 3C, with a few cells in layer 4α (arrow). Arrowheads mark the positions of CO blobs. Cells tend to cluster underneath CO blobs. **B:** Photomicrograph of a section from owl monkey 96-41, cut transverse to the cortical layers. Cells are confined to the CO-pale layer 3C, and tend to cluster beneath the blobs (arrowheads). **C:** A higher power view of MT-projecting cells in the bush baby. Cells in layer 3C tend to be larger than those in the upper parts of layer 3; well-labeled apical dendrites can be seen on both types of cells. Note the row of CO-dense cells in the middle of layer 5. One of these (arrow) also contains retrogradely transported tracer. **D:** A tangential section from bush baby 96-30. The plane of the section passes through layer 3B in the middle of the photomicrograph, going progressively lower through layer 3C toward the right, and into layer 4 (dashed line) at the right edge of the micrograph. The arrows mark three blobs in which labeled neurons are clearly clustered. **E:** A tangential section from owl monkey 96-38. Most of the micrograph is within layer 3C, where blobs are visible, albeit not as clearly as in layer 3B. Three blobs are marked by arrows. The density of labeled cells is greater within the blobs. Scale bars = 1 mm in A, B; 500 μm in C–D.

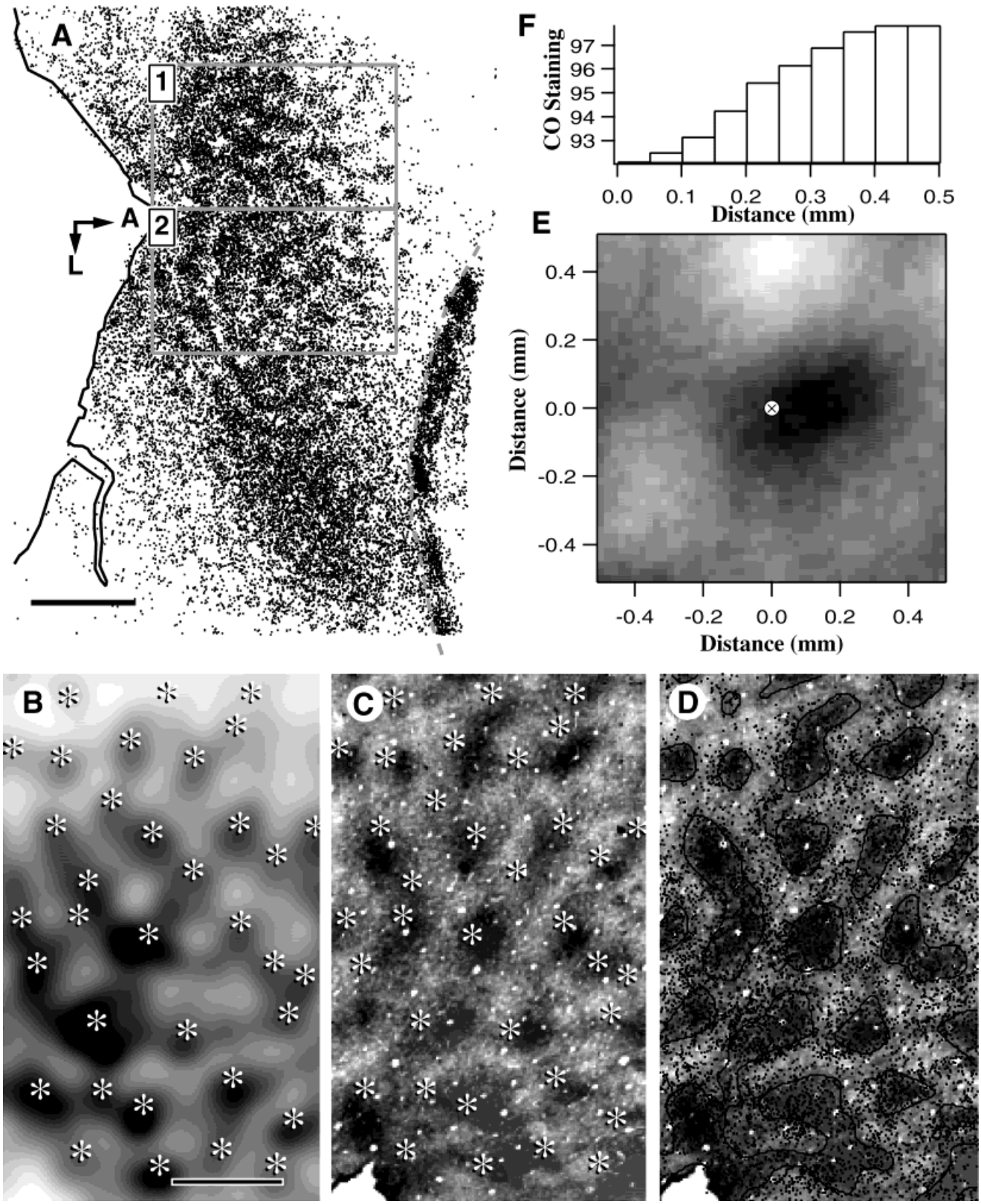
A
1
2
A
L
F
CO Staining
97
96
95
94
93
0.0
0.1
0.2
0.3
0.4
0.5
Distance (mm)
E
0.4
0.2
0.0
-0.2
-0.4
Distance (mm)
-0.4
-0.2
0.0
0.2
0.4
Distance (mm)
B
C
D

Figure 3

TABLE 1. Chi-Square Analyses of MT-Projecting Cells and CO Compartments[1]

Experiment	Species/ layer	Blob labeling density (cells/mm^2)	Interblob labeling density (cells/mm^2)	Border labeling density (cells/mm^2)	*P*-value
95_33	Bush baby/3	568	380	492	$P < 0.001$
95_32	Bush baby/3	338	211	254	$P < 0.001$
96_30	Bush baby/3	297	150	199	$P < 0.001$
96_17	Owl monkey/3	1,780	1,322	1,533	$P < 0.001$
96_38	Owl monkey/3	845	610	690	$P < 0.001$
96_41	Owl monkey/3	647	442	507	$P < 0.001$
95_33	Bush baby/5	62	58	57	$P > 0.05$
95_32 (box 2)	Bush baby/5	19	15	17	$P > 0.05$
96_38 (box 2)	Owl monkey/6	4.5	5.5	4.4	$P > 0.05$
Shipp and Zeki (1989)	Macaque/4B	17.2	8.3	15.9	$P < 0.01$

[1]CO, cytochrome oxidase; MT, middle temporal area.

sponds to the average CO staining density at that distance from the MT-projecting cells. The dark area in the center of the image indicates that MT-projecting cells are found preferentially in areas of darker CO staining. The size and spacing of the dark area in the center of the image, and the dark areas along the edges of the image (caused by the regular periodicity of the CO blobs; they represent the average position of adjacent blobs) are the same as the size and spacing of the CO blobs, showing the relationship between the MT-projecting cells and the CO architecture. The fact that the dark area is not centered exactly on the reference position is probably caused by imprecision in aligning the MT-projecting cells with the CO image, which was taken from a section more superficial in the cortex than the sections containing most of the labeled cells.

The two-dimensional cross-correlation in Figure 3E was collapsed radially onto a single dimension and divided into 0.05-mm bins, giving the plot shown in Figure 3F—where the average CO staining value is plotted as a function of distance from the reference position. The CO staining value is lowest (darker staining) closest to the reference position, and gradually increases, leveling off at about 0.4 mm away from the reference position. Note that although the original CO image was an 8-bit image, i.e., it had values ranging from 0–255, the range of values in the correlation result is much smaller due to the averaging involved.

Analyses of the relationship between CO staining and retrogradely-labeled MT-projecting cells was carried out in the same fashion for two other bush baby cases: 95–32 and 96–30. The results from case 95–32 is shown in Figure 4, which has the same format as Figure 3.

Figure 4A shows the reconstruction of retrogradely labeled cells. The density of labeling in this experiment was not as great as in the case shown in Figure 3, but the patchiness of the labeling is just as apparent. As in Figure 3, two boxes were chosen for analysis. The results from box 1 are shown in detail in Figure 4B–D. In this case, the match between the patches of MT-projecting cells (Fig. 4A) and CO blobs (Fig. 4B) appears as good, or better, than the case shown in Figure 3.

Most patches of MT-projecting cells correspond to a CO blob. Figure 4D shows the CO staining pattern, with blobs outlined, and the pattern of retrogradely labeled cells; the results of the χ^2 analysis for this experiment are shown in row 2 of Table 1. The cross-correlation analysis is shown in Figure 4D,E. There is a dark area in the center of the two-dimensional cross-correlation image (Fig. 4E), centered on the reference position, and there are secondary dark areas at the edge of the plot.

One other bush baby hemisphere was also analyzed (96–30; not shown). The data and analysis from this experiment were in agreement with the data presented in Figures 3 and 4. The results from the χ^2 analysis of these data are shown on line 3 of Table 1.

Owl monkey layer 3. Three owl monkey hemispheres were analyzed in the same fashion as was done for the bush babies. Figure 5 shows the results for case 96–17; Figure 6 shows the results for case 96–38; and Figure 7 shows the results for case 96–41. Figures 5A, 6A, and 7A show the reconstructions of the labeling patterns in V1 for the three cases. Labeling also was found in V2 of these animals; only labeling in V2 near the V1/V2 border was charted, so label in V2 was much more extensive than is shown here. Labeling was present over a larger area of cortex in V1 in the owl monkeys than in the bush babies, as larger injections were made in the owl monkeys, and the fact that V1 is larger in owl monkeys than in bush babies. Labeling in V1 tended to be denser in the owl monkeys, with approximately twice as many cells/mm^2 in both blob and interblob compartments as were found in bush babies (possibly due to the larger injections). In the reconstructions, the clusters of MT-projecting cells do not appear to be as patchy as they do in bush babies, although nearer the edges of the labeled areas the patchy pattern is clearer. This edge effect is shown clearly in Figure 5A from case 96–38. In this case, the area chosen for analysis was taken from near the edge of the labeled zone. This difference in patchiness between the edges and the centers of the labeled areas may reflect actual differences in the specificity of the connections, but the appearance of patchiness might also be caused by the difference in labeling density between the center and edges; when Gaussian smoothed images of the MT-projecting cells were made (Figs. 5B, 6B,

Fig. 3. Results from bush baby case 95-33. **A:** Surface view of middle temporal (MT) projecting cells in the primary visual cortex (V1) composited from charts of retrograde labeling in a series of tangential sections through layers 2–4. The thick solid line shows the edge of the section, where the cortex was cut through the depths of the calcarine fissure to enable flattening. The thick gray dashed line indicates the border between V1 and secondary visual cortex (V2). Boxed area number 1 corresponds to the enlarged area shown in Figure 5B. **B:** A Gaussian smoothed image generated from the data from the boxed area shown in A. Darker areas correspond to higher densities of cells. An asterisk was placed over patches of high cell density, for comparison with cytochrome oxidase (CO) blobs shown in C. **C:** CO image from a superficial section, aligned with the data from B using blood vessels as landmarks. The asterisks show the same locations as in B. Note that most of the asterisks are over or near a CO blob. **D:** The same CO image as shown in C, with the positions of the labeled neurons represented by black dots. The borders of the CO blobs are indicated by solid lines. Blob and interblob borders were determined using the procedure described in the text for box 1 and box 2 and the results from both boxes were combined to give the χ^2 statistic shown in line 1 of Table 1. **E:** The two-dimensional spatial cross-correlation of the data shown in B and C. The darkness of the image at each x–y offset is proportional to the density of CO staining at that offset averaged over all the labeled cells. The dark spot at the origin of the plot (marked with cross-hairs) shows that CO staining was darker near labeled cells. The dark spot matches—in average size (approximately 0.3-mm diameter), shape, and orientation (elongated obliquely)—that of the CO blobs in C–D, indicating that the CO blobs are responsible for the observed correlation. **F:** The one-dimensional spatial correlation between distance from labeled cells and CO staining density. Scale bars = 2.0 mm in A; 1.0 mm in B–D.

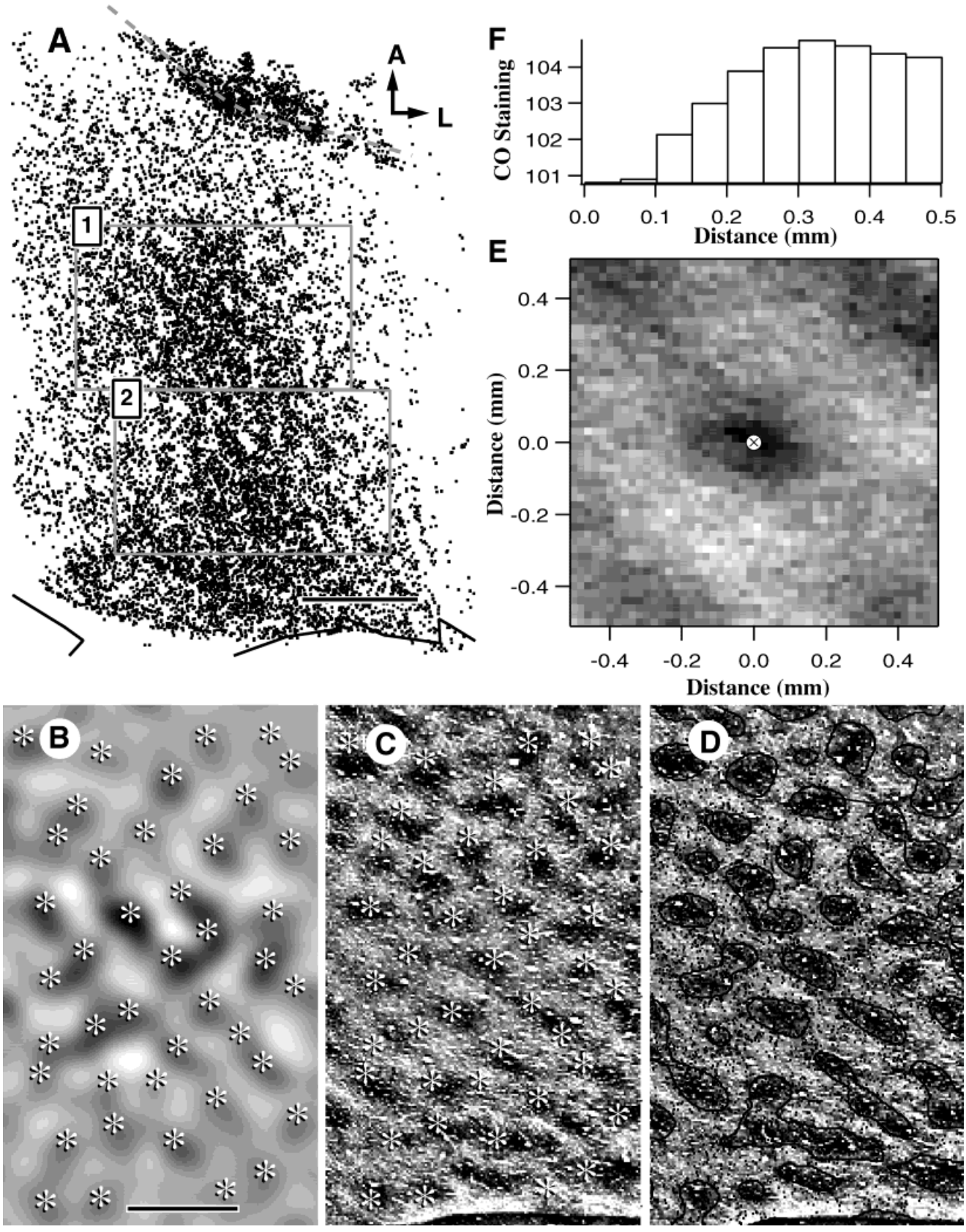

Fig. 4. Results from bush baby case 95-32. The labeling conventions are as in Figure 3, except that the cortical axes of the plot of labeled cells in **A** is rotated 90°. The data from box number 1 are shown in **B–F.** The combined χ^2 analysis for both boxes is shown on line 2 of Table 1. The results in B–C show good correspondence between the patches of middle temporal area (MT) projecting cells and the cytochrome oxidase (CO) blobs. Note that the dark spot at the center of the two-dimensional spatial correlation plot in E is centered on the reference point, showing that the cells tend to align with the darkly staining CO blobs. Scale bars = 2.0 mm in A; 1.0 mm in B–D.

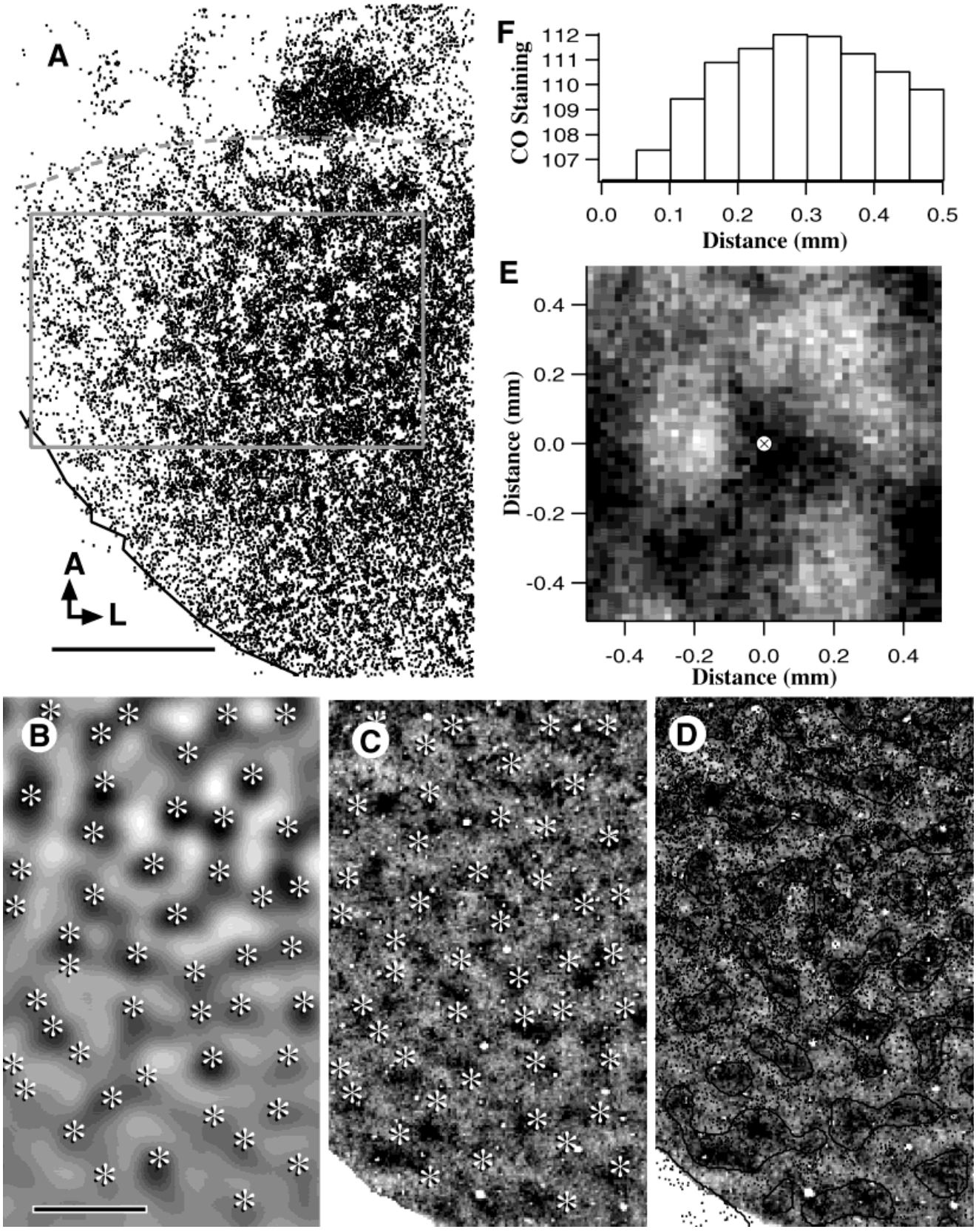

Fig. 5. Results from owl monkey case 96-17. Same conventions as in Figure 3. **A:** A reconstruction of the middle temporal area (MT) projecting cells from near the edge of the area containing retrograde labeling. Figures **B** and **C** show that the patches of labeled cells tend to correspond with the positions of cytochrome oxidase (CO) blobs, and cross-correlation plots (**E, F**) show that MT-projecting cells tended to be found near darker CO staining. The χ^2 analysis for these data (**D**) is on line 4 of Table 1. Scale bars = 2.0 mm in A; 1.0 mm in B–D.

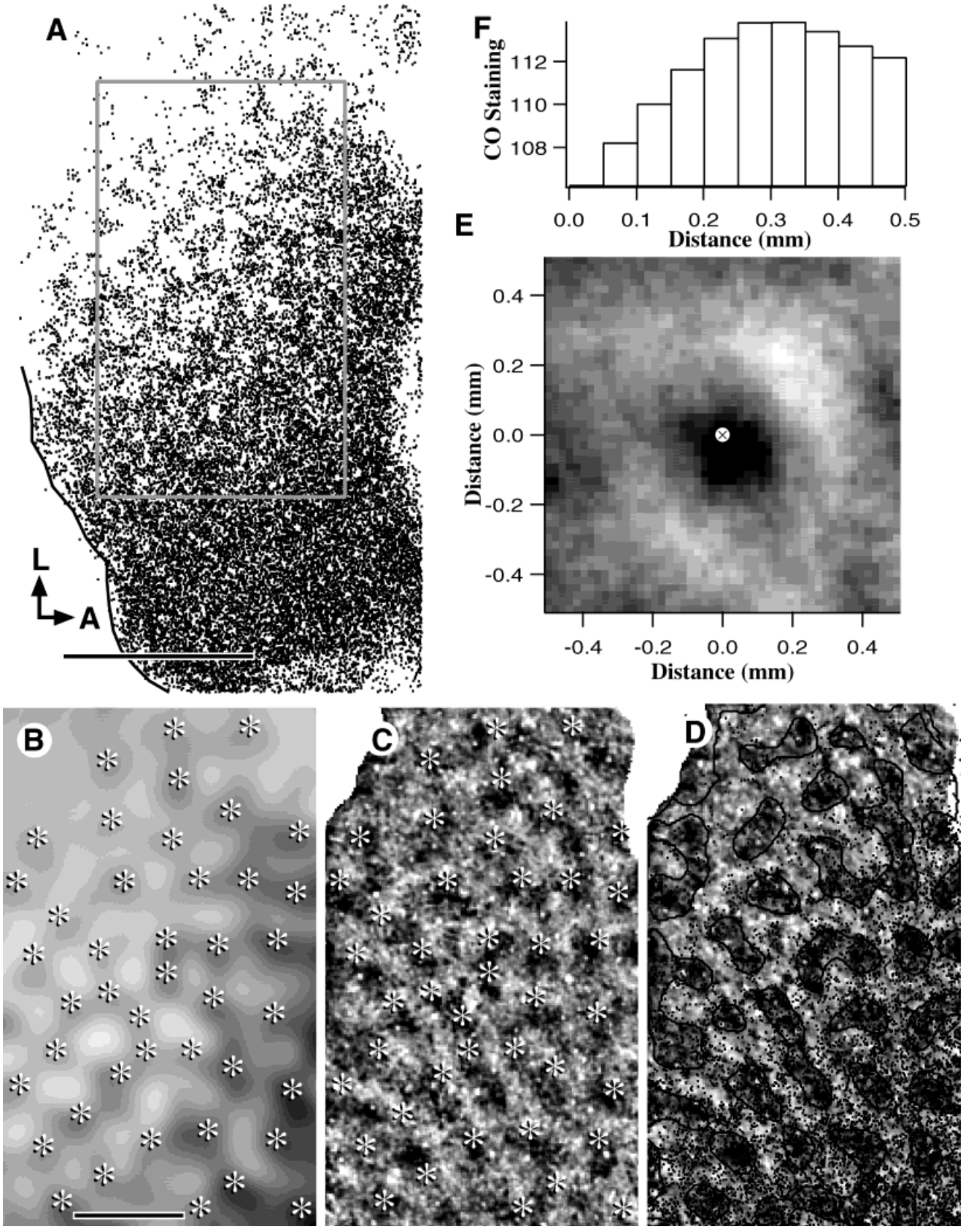

Fig. 6. Results from owl monkey case 96-38. Same conventions as in Figure 3. The reconstruction of labeling (**A**) is not as clearly patchy as in the other two cases, but the correspondence between middle temporal area (MT) projecting cells and cytochrome oxidase (CO) blobs is visible when the Gaussian image (**B**) is compared to the CO-stained section (**C**), and the cross-correlation plots (**E, F**) show dark CO staining near MT-projecting cells. The χ^2 analysis for these data is (**D**) on line 5 of Table 1. Scale bars = 2.0 mm in A; 1.0 mm in B–D.

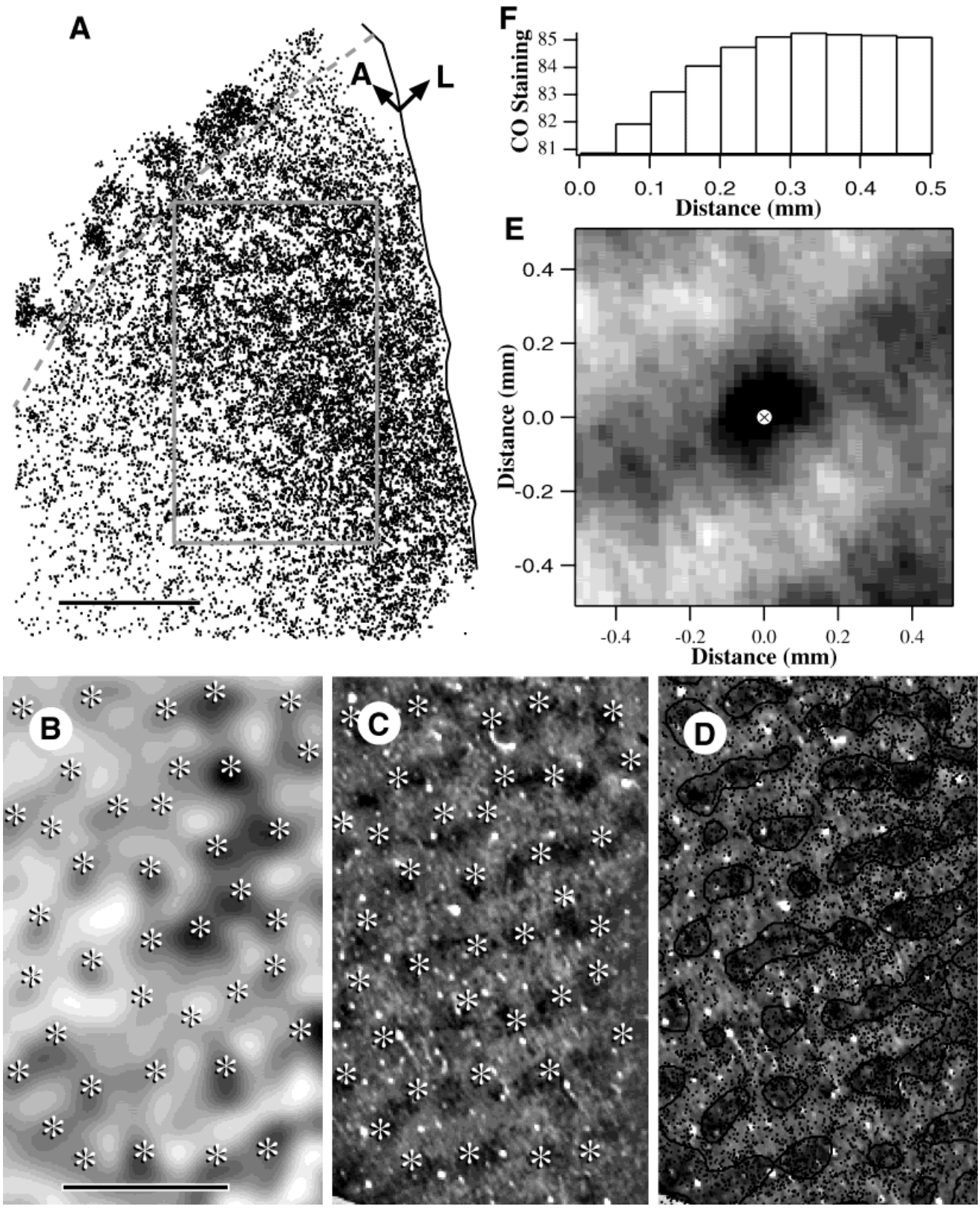

Fig. 7. Results from owl monkey case 96-41. Some conventions as in Figure 3. The χ^2 analysis for these data is on line 6 of Table 1. Scale bars = 2.0 mm in A; 1.0 mm in B–D.

7B), the areas of densest labeling appeared as patchy as areas of less dense labeling near the edges.

Figure 5B–D show the relationship between the patches of MT-projecting cells and the CO architecture for case 96–17. In this case, the patchiness of the labeling near the center of the labeled zone was clearer than it was for the other two owl monkey cases. The correspondence between patches of MT-projecting cells and CO blobs is similar to that seen in the bush babies. Figure 5D shows the MT-projecting cells overlaid on the CO image, with the positions of the CO blobs used for the χ^2 analysis outlined. It appears that there is a higher percentage of retrogradely labeled cells outside the CO blobs than was the case for the bush babies, and this qualitative observation was confirmed quantitatively (line 4 of Table 1). Nevertheless, the density of MT-projecting cells within the CO blob compartment is still greater than in the interblob or blob border compartments, and this difference is significant. The results of the cross-correlation analyses in owl monkeys (Fig. 5 D,E) are similar to the findings in bush babies. The dark area centered on the reference position in Figure 5E shows that MT-projecting cells are found mainly in areas of dark CO staining, and the size and spacing of the dark areas on the correlation image are the same as the size and spacing of the CO blobs.

Figure 6B–D show the results for another owl monkey experiment, 96–38, again with good correspondence between the patches of MT-projecting cells and CO blobs. The results from the χ^2 analysis for this experiment, including another boxed area not illustrated, are shown on line 5 of Table 1. Again, the density of MT-projecting cells was significantly greater in the CO blob compartments. Figure 6E,F show the results of the cross-correlation analysis for these data. The dark area centered on the reference point is relatively rounded and regular, matching the round, regular appearance of the CO blobs in Figure 6D.

Another owl monkey case (96–41) was analyzed in the same fashion with similar results (Fig. 7). Although this case does not appear as patchy as the other cases when looking at the pattern of labeled cells (Fig. 7A), the patches actually are more visible in the Gaussian smoothed image (Fig. 7B), and these patches align very well with the blobs in the CO-stained section (Fig. 7C). The results from the χ^2 analysis for this animal (Fig. 7D) are presented on line 6 of Table 1. The two-dimensional cross-correlation image for these data (Fig. 7E) shows a dark spot centered on the reference point, and the other dark spots representing the position of adjacent blobs have the same shape and orientation as the blobs in the original CO image (Fig. 7C).

Bush baby and owl monkey: Infragranular layers. In addition to the cells in layer 3, there was a minor population of MT-projecting cells located in the deeper layers (layer 5 for bush babies and layer 6 for owl monkeys). As we took several of the deeper sections for myelin staining, it is very likely that MT-projecting cells from the infragranular layers were under-represented. Also, aligning sections from the deeper cortical layers with superficial CO-stained sections is more problematic than for the layer 3 labeling. The retrograde labeling in the deeper layers was analyzed separately from the cells in layer 3. Figure 8A shows the MT-projecting cells in layer 5 from bush baby 95–33 from box 1 in Figure 3A. Compare this figure with Figure 3D, which shows the layer 3 MT-projecting cells from the same part of V1. There are approximately 10% as many retrogradely labeled cells in layer 5 as there are in layer 3. The χ^2 analysis of the combined data from the two boxes analyzed in this experiment (line 7 of Table 1) showed that, although MT-projecting cells in layer 5 were slightly more numerous in blob compartments, it was not a significant departure from the distribution that would be expected from chance alone. The cross-correlation analysis from these data are shown in Figure 8B,C. There is a slight suggestion of greater density in a region offset to the upper left of the reference point; the offset could be a result of imprecision in aligning the labeling with superficial CO-stained tissue. However, there is no prominent dark area in the center of the cross-correlation image, as was found in the analysis of the cells from layer 3. A second example of layer 5 MT-projecting cells and CO staining (bush baby 95–32; box 2 of Fig. 4) is shown in Figure 8D–F. The χ^2 analysis of these data is shown on line 8 of Table 1 (the area corresponding to box 1 in Figure 4 contained too few MT-projecting cells in layer 5 to analyze). Again, there were slightly, but not significantly, more cells in blobs than in interblobs. The cross-correlation image shows a pattern which, although much less robust than the patterns obtained from the much more numerous layer 3 neurons, is somewhat similar in organization—suggesting a slight tendency for cells to be located under blobs.

In owl monkey, MT-projecting cells in layer 6 were much less than 1% as numerous as MT-projecting cells in layer 3. In only one owl monkey (96–38) was there a large enough population of layer 6 cells labeled to attempt an analysis. The results from the χ^2 analysis of this case are given in line 9 of Table 1. There were slightly fewer labeled cells under blobs than under interblobs, but this was not significant statistically.

DISCUSSION

In these experiments, we investigated the tangential organization of cells in V1 projecting to the middle temporal area (MT). We found that MT-projecting cells were unevenly distributed across the surface of the cortex, with patches of dense labeling separated by regions of less dense labeling. Moreover, the patches of dense labeling tended to lie beneath the CO blobs. These results show that CO blob columnar differences are also present below these compartments, and can also be demonstrated within layer 3C.

Robustness of the finding

It is important to emphasize that like the periodicity of the CO blobs and interblobs, the patches and interpatches of cells projecting to MT resemble a sine wave rather than a square wave gradient, with peaks having 1.5 to 2 times greater density than the valleys. It would be interesting to compare the strength of the relationship of CO staining and MT-projecting cells to that of the relationship of CO staining and other projection cell populations that are known to be related to CO blob compartments. Unfortunately, few studies have employed quantitative measures, although the relationship of CO blobs and corticotectal cells obtained in a recent study (Abel et al., 1997) showed a similar strength (about 1.5 times greater density of cells under one compartment than in the other). Although not quantified, it would appear from visual inspection of published figures (Livingstone and Hubel, 1983) that the relationship of CO blobs and cells projecting to different

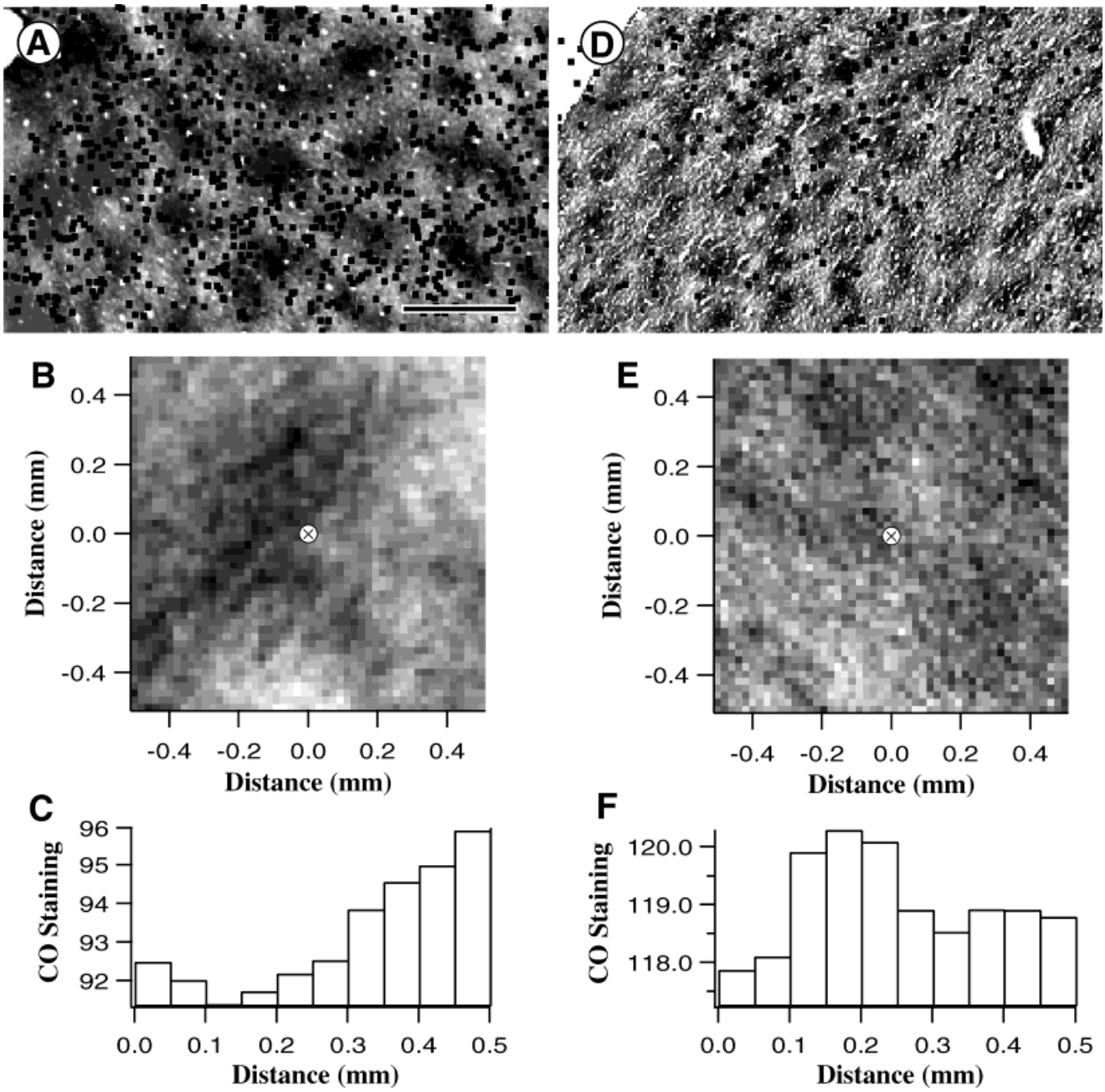

Fig. 8. Results from the analysis of labeled layer 5 cell distributions in bush baby. The results for case 95-33 are shown in **A–C.** These data are from the boxed area marked number 1 in Figure 3. Chi-square analysis for these data is shown on line 7 of Table 1. The results from case 95-32 are shown in **D–F** and on line 8 of Table 1. These data are from box 2 in Figure 4. There is no apparent relationship between middle temporal area (MT) projecting cells in layer 5 and cytochrome oxidase (CO) blobs.

compartments of V2 might be a good deal stronger than this; i.e., following an injection confined to a single thin stripe in V2, the ratio of the density between blob and interblob compartment labeling appears to be greater than the 1.5 to 2 times seen here. Of course, the V2-projecting cells are found in different layers (3A,B) than the MT-projecting cells, and it is possible that intercompartmental differences generally are more pronounced in layers 3A and 3B than they are in layer 3C. It would be interesting to compare the relationship to the CO architecture of the different populations of projection cells within a single layer, free from the confounds of laminar location. Layer 3C makes projections to other cortical areas in addition to MT, such as the thick stripes of V2 (Livingstone and Hubel, 1987) and the dorsal medial visual area (DM) (Krubitzer and Kaas, 1990a; Vogt Weisenhorn et al., 1995). In owl monkeys and bush babies (but not squirrel monkeys or macaque monkeys), cells within CO-blob columns project more heavily to the Dorsal Medial (DM) visual area than cells in the interblob columns (Beck and Kaas, 1998a,b, in

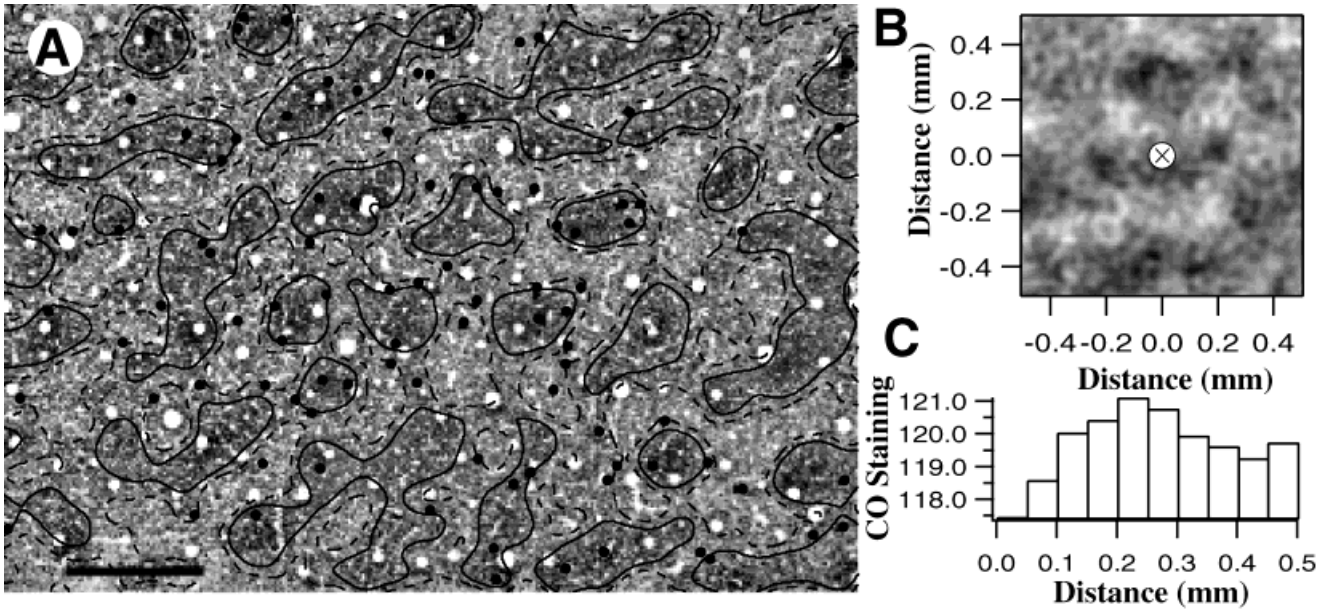

Fig. 9. Reprinted from Shipp and Zeki (1989) with permission from Blackwell Publishers. Their figure 11 showing the arrangement of cytochrome oxidase (CO) blobs and middle temporal (MT) projecting cells (black dots) in macaque monkey was scanned (**A**) and then analyzed as for the other data in this paper. The boundaries between CO blobs and border regions, determined using the procedure described in the text, are indicated by solid lines; the boundaries between interblobs and border regions are shown in dashed lines. These data were used to calculate the χ^2 statistic shown in line 10 of Table 1. When CO compartments are defined quantitatively thusly, there is a significantly higher density of MT-projecting cells in the blobs versus the interblobs. The spatial cross-correlations plots, **B** and **C**, show that labeled cells tended to be found in areas of darker CO staining. Scale bar = 0.5 mm in A.

press). As cells in both 3B and 3C project to area DM, it would be interesting to compare the degree to which the DM-projecting cells in different layers (3B versus 3C) are concentrated in the blob columns.

Comparative aspects

It is interesting to compare the results in this study using bush babies and owl monkeys to a recent study in macaque monkeys, which obtained somewhat different results (Shipp and Zeki, 1989). In contrast to the present study, the MT-projecting cells in layer 3C of macaque monkey reportedly showed no relationship to the overlying CO blobs. The differences in the results between their study and ours could be due to real differences between the three species and/or technical differences between the two studies. The labeling density is certainly much lower in macaque monkey V1 than in owl monkey or bush baby, making quantitative analysis more difficult. Equally important, the methods of defining blobs boundaries for the χ^2 analysis differed; whereas blobs in this study were defined as occupying about one-third of the cortex, the blobs outlined by Shipp and Zeki occupied only about 15% of the cortical area.

To help resolve this issue, we analyzed data from Ship and Zeki's paper (their figure 11) using our method of dividing the cortical surface into three equal sized compartments of blobs, interblobs, and border regions. Figure 9A shows our blob and interblob boundaries superimposed on the original CO staining image and cell positions. The χ^2 analysis of this figure shows that the density of cells is more than twice as great in blobs as it is in interblobs. Even though the absolute number of cells is quite small, the deviation of the distribution from chance is statistically significant at the 0.01 level. Figure 9B and C show the results of the spatial cross-correlation, which also suggest that labeled cells tend to be found in CO blobs. Thus, it would appear that the organization of MT-projecting cells in layer 3 is consistent across different primate species.

In a similar manner, we analyzed Shipp and Zeki's figure 13a, comparing the positions of layer 6 cells projecting to MT with the CO architecture (not shown). Here, the results of our methods agreed with Shipp and Zeki's conclusion that MT-projecting cells in layer 6 cell tend to be less common below CO blobs. We have also analyzed published data on corticotectal cells and CO blobs (Lia and Olavarria, 1996) with a similar result. Thus, our methods are able to show instances of cell populations avoiding CO blobs, as well as populations that concentrate in CO blobs.

Surprisingly, Shipp and Zeki found that terminal labeling in layer 3C was strikingly patchy, but was not aligned with the overlying CO blobs. Also, injections into MT of tritiated amino acids, a strictly anterograde tracer, did not give patchy labeling in 3C (Maunsell and Van Essen, 1983; Ungerleider and Desimone, 1986; Shipp and Zeki, 1989), suggesting that the patches seen by Shipp and Zeki were the result not of projections from MT but were the result of labeling the collaterals of cells that were retrogradely labeled from MT. We did not examine terminal labeling in the present experiments, as CTB-Au, in our hands, was a strictly retrograde tracer, with no anterograde or collateral transport. Therefore, we do not know if feedback projections from MT in the owl monkey and bush baby would colocalize with the patches of cells that project to MT in the blob columns. Shipp and Zeki (1989) suggested that the patches of terminal labeling marked another columnar

system, with a similar periodicity to the CO blobs, but organized independently of them.

Interesting differences can be seen comparing the prosimian bush baby to the New World simian owl monkey and the Old World simian macaque monkey. In bush baby, as noted by Condo and Casagrande (1990), dense CO staining exists from the CO blobs in layer 3B all the way to the top of layer 4, without an intervening CO-pale layer (3C), at least in heavily stained sections. The MT-projecting cells mirror this lack of a well-defined 3C by being less confined than in the simian primates to a single layer; instead, MT-projecting cells extend some distance up into layer 3B (Diamond et al., 1985; present study), and are occasionally found in the upper part of layer 4 (present study). In both owl and macaque monkeys, layer 3C is CO pale, and MT-projecting cells (aside from the few cells in layers 5/6) are confined to layer 3C. However, CO blob/interblob distinctions appear qualitatively to be more obvious in owl monkey layer 3C than in macaque monkey layer 3C. Thus, one possibility is that the degree to which the MT-projecting cells are clustered in the blobs is proportional to the contrast between blobs and interblob compartments in the CO staining at the laminar level in which the cells are found, although the functional significance of such correlations remains obscure.

Labeling in the infragranular layers also showed an interesting species difference. In macaque monkey, MT-projecting cells in the supergranular layers are a subset of Meynert cells (Lund et al., 1975; Fries et al., 1985), and Meynert cells have been shown to be more numerous under interblobs than blobs (Fries, 1986; Payne and Peters, 1989). Not surprisingly, the MT-projecting Meynert cells have also been shown to be more numerous under interblobs than blobs (Shipp and Zeki, 1989). In the prosimian bush baby, however, we found that, if anything, MT-projecting cells in the infragranular layers were more numerous under blobs. It is hard to comment on the significance of this difference, as it is not yet known if the entire population of large, CO-reactive layer 5 cells, of which the ones projecting to MT form a only subset, have the same spatial relationship to the blobs as Meynert cells do in simians. We also do not have enough data on owl monkey layer 6 cells to tell if they follow the same pattern as the equivalent cells in the macaque monkey.

Functional considerations

Area MT is an extrastriate area which is generally agreed to be concerned with motion processing in both macaque monkeys (Zeki, 1974; Albright, 1984, 1992; Boussaoud et al., 1990) and owl monkeys (Allman et al., 1981; Felleman and Kaas, 1984). The cells projecting from V1 to MT are found in layers 3C and 6, which are the layers containing the highest proportion of directionally selective cells in macaque monkeys (Blasdel and Fitzpatrick, 1984) and bush babies (DeBruyn et al., 1993), although it has been reported that direction selectivity may be less confined in New World primates (Sengpiel et al., 1996; O'Keefe et al., 1998). A recent study using antidromic activation has confirmed that the V1 neurons projecting to MT are direction-selective in macaque monkeys (Movshon and Newsome, 1996). In all primate species, the MT-projecting cells in layer 3C are just above the terminations of the magnocellular geniculate inputs (Tigges et al., 1981; Diamond et al., 1985; Shipp and Zeki, 1989).

The laminar location of magnocellular inputs and MT-projecting cells in V1 apparently allows for the generation of a segregated direction-selective, magnocellular-driven output to MT. But if the circuitry within a layer alone is sufficient to account for the generation of the response properties of MT-projecting cells, why are these cells clustered below the CO blobs? One possibility is that circuitry relating to blob/interblob differences might also be involved in generating the properties of MT-projecting cells. The best example of inputs specific to the blobs are the koniocellular layers of the LGN, which project to layer 3B of the blobs in all primates examined (Livingstone and Hubel, 1982; Fitzpatrick et al., 1983; Diamond et al., 1985; Lachica and Casagrande, 1992; Hendry and Yoshioka, 1994; Ding and Casagrande, 1997). Because koniocellular axons arborize directly above the MT-projecting cells, these axons might be expected to terminate on the their apical dendrites. The physiological properties of these koniocellular cells are different from magnocellular and parvocellular LGN cells, and, at least in bush babies, where they have been most closely examined, are similar to W-cells found in other species (Irvin et al., 1986). Because koniocellular cells, unlike magnocellular or parvocellular cells, receive strong projections from the superior colliculus (Harting et al., 1986, 1991), it has been suggested that the koniocellular geniculocortical projection may be involved in saccadic suppression, or other functions related to eye movements (Casagrande, 1994). Eye movement-related modulation of information passing from V1 to MT would be logical, given the preference of neurons in MT for moving stimuli (Zeki, 1974; Albright, 1984) and the fact that eye movements can be elicited by electrical stimulation of MT (Jampel, 1960).

It is also possible that the magnocellular geniculate inputs to layer 4α below blobs and interblobs may be different. This is suggested by the fact that CO staining in bush babies (Condo and Casagrande, 1990) and owl monkeys (Horton, 1984) is not uniform in this layer; rather, dense and light patches in register with the blobs and interblobs in layer 3B can be distinguished. In macaque monkeys, CO staining in 4α appears uniform in adults, but a similar patchy pattern similar to that seen in owl monkeys and bush babies can be seen early in development (Horton, 1984). It may be that the magnocellular input to layer 4α below the blobs differs from that to layer 4α below the interblobs, either quantitatively or qualitatively. Compared to parvocellular LGN cells, magnocellular LGN cells in macaque monkeys (Kaplan and Shapley, 1982; Hubel and Livingstone, 1990), owl monkeys (Sherman et al., 1976), and bush babies (Norton and Casagrande, 1982) have larger receptive fields and higher contrast sensitivity and respond better to lower spatial frequencies and more rapidly moving stimuli. It has often been suggested that magnocellular neurons are particularly important for the discrimination of movement (for review, see Merigan et al., 1991). Inactivation of the magnocellular or parvocellular geniculate layers shows that responses in MT are dependent mainly on magnocellular, but not parvocellular, inputs channeled through V1, at least in macaque monkeys (Maunsell et al., 1990; Allison et al., 1995). Anatomical tracing experiments also show that layer 3C in all primates examined receives its main intracortical input from layer 4α (Lachica et al., 1992, 1993; Yoshioka et al., 1996). Thus, it appears that the main input to MT comes from the magnocellular layers

of the LGN and passes through V1. The fact that MT-projecting cells are clustered below the CO-blobs leads to the hypothesis that the transfer of information from magnocellular layers of the LGN through V1 to MT is preferentially through the CO blob columns. This suggests that the magnocellular input to layer 4α beneath CO blobs is distinct from magnocellular input to layer 4α beneath interblobs either quantitatively or qualitatively.

ACKNOWLEDGMENTS

This study was supported by NIH grant EY01778 to VAC, and core grants EYO8126 and HD15051. We thank Amy Nunnally for assistance in surgery, Julia Mavity-Hudson for help with the histology, Paul Matrisian for providing access to computer facilities, and Dr. Jon Kaas for comments on the manuscript. We also thank Dr. Alan Saul for advice on creating some of the analysis routines used in this paper and Dr. Jan Romergy for proofing the manuscript.

LITERATURE CITED

Abel PA, O'Brien BJ, Lia B, Olavarria JF. 1997. Distribution of neurons projecting to the superior colliculus correlates with thick cytochrome oxidase stripes in macaque visual area 2. J Comp Neurol 377:313–323.

Albright TD. 1984. Direction and orientation selectivity of neurons in visual area MT of the macaque. J Neurophysiol 52:1106–1130.

Albright TD. 1992. Form-cue invariant motion processing in primate visual cortex. Science 255:1141–1143.

Allison JD, Melzer P, Ding Y, Dinger J, Bonds AB, Casagrande VA. 1995. The contribution of LGN M and P layers to the contrast sensitivity of primate V1 neurons. Soc Neurosci Abstr 21:394.

Allman JM, Kaas JH. 1971. A representation of the visual field in the caudal third of the middle temporal gyrus of the owl monkey (*Aotus trivirgatus*). Brain Res 31:85–105.

Allman JM, Kaas JH. 1974. A crescent-shaped cortical visual area surrounding the middle temporal area (MT) in the owl monkey (*Aotus trivirgatus*). Brain Res 81:199–213.

Allman JM,. Kaas JH, Lane RH. 1973. The middle temporal visual area (MT) in the bushbaby (*Galago senegalensis*). Brain Res 57:197–202.

Allman JM, Baker JF, Newsome WT, Peterson FE. 1981. Visual topography and function: cortical visual areas in the owl monkey. In: Woolsey CN, editor. Multiple visual areas. Clifton, NJ: Humana Press, Inc. p 171–185.

Beck PD, Kaas JH. 1998a. Cortical connections of the dorsomedial visual area in New World owl monkeys (*Aotus trivirgatus*) and squirrel monkeys (*Saimiri sciureus*). J Comp Neurol 400:18–34.

Beck PD, Kaas JH. 1998b. Cortical connections of the dorsomedial visual areas in prosimian primates. J Comp Neurol 398:162–178.

Beck PD, Kaas JH. 1999. Cortical connections of the dorsomedial visual areas in Old World macaque monkeys. J Comp Neurol. (in press)

Blasdel GG, Fitzpatrick D. 1984. Physiological organization of layer 4 in macaque striate cortex. J Neurosci 4:880–895.

Boussaoud D, Ungerleider LG, Desimone R. 1990. Pathways for motion analysis: Cortical connections of the medial superior temporal and fundus of the superior temporal visual areas in the macaque. J Comp Neurol 296:462–495.

Boyd JD, Casagrande VA. 1996. Modular architecture of cells projecting from primary visual cortex (V1) to area MT. Soc Neurosci Abstr 22:640.

Boyd JD, Matsubara JA. 1996. Laminar and columnar patterns of geniculocortical projections in the cat: relationship to cytochrome oxidase. J Comp Neurol 365:659–682.

Brodmann K. 1909. Vergleichende lokalisationlehre der grosshirnrinde in ihren prinzipien dargestelt auf des zellenbaues. Leipzig: JA Barth.

Casagrande VA. 1994. A third parallel visual pathway to primate area V1. TINS 17:305–310.

Casagrande VA, Kaas JH. 1994. The afferent, intrinsic, and efferent connections of primary visual cortex in primates. In: Peters A, Rockland KS, editors. Cerebral cortex. New York: Plenum Press. p 201–259.

Chan-Palay VS, Palay SL, Billings-Gagliardi SM. 1974. Meynert cells in the primate visual cortex. J Neurocytol 3:631–658.

Condo GC, Casagrande VA. 1990. Organization of cytochrome oxidase staining in the visual cortex of nocturnal primates (*Galago crassicaudatus* and *Galago senegalensis*): I. Adult patterns. J Comp Neurol 293:632–645.

DeBruyn EJ, Casagrande VA, Beck PD, Bonds AB. 1993. Visual resolution and sensitivity of single cells in the primary visual cortex (V1) of a nocturnal primate (bush baby): correlation with cortical layers and cytochrome oxidase patterns. J Neurophysiol 69:3–18.

DeYoe EA, Felleman DJ, Van Essen DC, McClendon E. 1994. Multiple processing streams in occipitotemporal visual cortex. Nature 371:151–154.

DeYoe EA, Van Essen DC. 1988. Concurrent processing streams in monkey visual cortex. TINS 11:219–226.

Diamond IT, Conley M, Itoh K, Fitzpatrick D. 1985. Laminar organization of geniculocortical projections in *Galago senegalensis* and *Aotus trivirgatus*. J Comp Neurol 242:584–610.

Ding Y, Casagrande VA. 1997. The distribution and morphology of LGN K pathway axons within the layers and CO blobs of owl monkey V1. Visual Neurosci 14:691–704.

Felleman DJ, Kaas JH. 1984. Receptive-field properties of neurons in middle tempoal visual area (MT) of owl monkeys. J Neurophysiol 52:488–513.

Fitzpatrick D, Itoh K, Diamond IT. 1983. The laminar organization of the lateral geniculate body and the striate cortex in the squirrel monkey (*Saimiri sciureus*). J Neurosci 3:673–702.

Fries W. 1986. Distribution of Meynert cells in primate striate cortex. Spatial relationships with cytochrome oxidase blobs. Naturwissenschaften 73:557–558.

Fries W, Keizer K, Kuypers HGJM. 1985. Large layer VI cells in macaque striate cortex (Meynert cells) project to both superior colliculus and prestriate visual area V5. Exp Brain Res 58:613–616.

Gallyas F. 1979. Silver staining of myelin by means of physical development. Neurol Res 1:203–209.

Harting JK, Hashikawa T, Van Lieshout D. 1986. Laminar distribution of tectal, parabigeminal and pretectal inputs to the primate dorsal lateral geniculate nucleus: connectional studies in *Galago crassicaudatus*. Brain Res 366:358–363.

Harting JK, Huerta MF, Hashikawa T, van Lieshout DP. 1991. Projection of the mammalian superior colliculus upon the dorsal lateral geniculate nucleus: organization of tectogeniculate pathways in nineteen species. J Comp Neurol 304:275–306.

Hässler R. 1967. Comparative anatomy of the central visual systems in day- and night-active primates. In: Hässler R, Stephen H, editors. Evolution of the forebrain. New York: Plenum Press. p 419–434.

Hendrickson AE. 1985. Dots, stripes and columns in monkey visual cortex. TINS 8:406–410.

Hendry SHC, Yoshioka T. 1994. A neurochemically distinct third channel in the macaque dorsal lateral geniculate nucleus. Science 264:575–577.

Horton JC. 1984. Cytochrome oxidase patches: a new cytoarchitectonic feature of monkey visual cortex. Phil Trans R Soc Lond B 304:199–253.

Horton JC, Hubel DH. 1981. Regular patchy distribution of cytochrome oxidase staining in primary visual cortex of macaque monkey. Nature 292:762–764.

Hubel DH, Livingstone MS. 1990. Color and contrast sensitivity in the lateral geniculate body and primary visual cortex of the macaque monkey. J Neurosci 10:2223–2237.

Irvin GE, Norton TT, Sesma MA, Casagrande VA. 1986. W-like response properties of interlaminar zone cells in the lateral geniculate nucleus of a primate (*Galago crassicaudatus*). Brain Res 362:254–270.

Jampel RS. 1960. Convergence, divergence, pupillary reaction and accommodation of the eyes from faradic stimulation of the macaque brain. J Comp Neurol 115:371–400.

Kaas JH, Morel A. 1993. Connections of visual areas of the upper temporal lobe of owl monkeys—the MT crescent and dorsal and ventral subdivisions of FST. J Neurosci 13:534–546.

Kaplan E, Shapely RM. 1982. X and Y cells in the lateral geniculate nucleus of macaque monkeys. J Physiol 294:561–580.

Krubitzer LA, Kaas JH. 1986. Cortical connections of MT and DL in the prosimian galago: Evidence that modular segregation of parallel pathways is a primitive feature in primates. Soc Neurosci Abstr 14:602.

Krubitzer L, Kaas J. 1990a. Convergence of processing channels in the extrastriate cortex of monkeys. Visual Neurosci 5:609–613.

Krubitzer LA, Kaas JH. 1990b. Cortical connections of MT in four species of primates: Areal, modular, and retinotopic patterns. Visual Neurosci 5:165–204.

Krubitzer LA, Kaas JH. 1993. The dorsomedial visual area of owl monkeys: Connections, myeloarchitecture, and homologies in other primates. J Comp Neurol 334:497–528.

Lachica EA, Casagrande VA. 1992. Direct W-like geniculate projections to the cytochrome oxidase (CO) blobs in primate visual cortex—axon morphology. J Comp Neurol 319:141–158.

Lachica EA, Beck PD, Casagrande VA. 1992. Parallel pathways in macaque monkey striate cortex: anatomically defined columns in layer III. Proc Natl Acad Sci USA 89:3566–3570.

Lachica EA, Beck PD, Casagrande VA. 1993. Intrinsic connections of layer-III of striate cortex in squirrel monkey and bush baby—correlations with patterns of cytochrome oxidase. J Comp Neurol 329:163–187.

Lia B, Olavarria JF. 1996. The distribution of corticotectal projection neurons correlates with the interblob compartment in macaque striate cortex. Visual Neurosci 13:461–466.

Lin CS, Weller RE, Kaas JH. 1982. Cortical connections of striate cortex in the owl monkey. J Comp Neurol 211:165–176.

Livingstone MS, Hubel DH. 1982. Thalamic inputs to cytochrome oxidase rich regions in monkey visual cortex. Proc Natl Acad Sci USA 79:6098–6101.

Livingstone MS, Hubel DH. 1983. Specificity of cortico-cortical connections in monkey visual system. Nature 304:531–534.

Livingstone MS, Hubel DH. 1984. Anatomy and physiology of a color system in the primate visual cortex. J Neurosci 4:309–356.

Livingstone MS, Hubel DH. 1987. Connections between layer 4B of area 17 and the thick cytochrome oxidase stripes of area 18 in the squirrel monkey. J Neurosci 7:3371–3377.

Lund JS, Lund RD, Hendrickson AE, Bunt AH, Fuchs AF. 1975. The origin of efferent pathways from the primary visual cortex, area 17, of the macaque monkey as shown by retrograde transport of horseradish peroxidase. J Comp Neurol 164:287–304.

Martin KAC. 1988. From enzymes to visual perception: a bridge too far? TINS 11:380–387.

Maunsell HR, Van Essen DC. 1983. The connections of the middle temporal visual area (MT) and their relationship to a cortical hierarchy. J Neurosci 3:2563–2586.

Maunsell JHR, Neally TA, DePriest DD. 1990. Magnocellular and parvocellular contributions to responses in the middle temporal visual area (MT) of the macaque monkey. J Neurosci 10:3323–3334.

Merigan WH, Byrne CE, Maunsell JHR. 1991. Does primate motion perception depend on the magnocellular pathway? J Neurosci 11:3422–34299.

Movshon JA, Newsome WT. 1996. Visual response properties of striate cortical neurons projecting to area MT in macaque monkeys. J Neurosci 16:7733–7741.

Norton TT, Casagrande VA. 1982. Laminar organization of receptive-field properties in lateral geniculate nucleus of bush baby (*Galago crassicaudatus*). J Neurophysiol 47:715–741.

O'Keefe LP, Levitt JB, Kiper DC, Shapley RM, Movshon JA. 1998. Functional organization of owl monkey lateral geniculate nucleus and visual cortex. J Neurophysiol 80:594–609.

Payne BR, Peters A. 1989. Cytochrome oxidase patches and Meynert cells in monkey visual cortex. Neuroscience 28:353–363.

Rodieck RW. 1991. The density recovery profile: A method for the analysis of points in the plane applicable to retinal studies. Visual Neurosci 6:95–111.

Rosa MGP, Schmid LM. 1995. Visual areas in the dorsal and medial extrastriate cortices of the marmoset. J Comp Neurol 359:272–299.

Sengpiel F, Troilo D, Kind PC, Graham B, Blakemore C. 1996. Functional architecture of area 17 of normal and monocularly deprived marmosets (*Callithrix jacchus*). Visual Neurosci 13:145–160.

Sherman SM, Wilson JR, Kaas JH, Webb SV. 1976. X- and Y-cells in the dorsal lateral geniculate nucleus of the owl monkey (*Aotus trivirgatus*). Science 192:475–476.

Shipp S, Zeki S. 1989. The organization of connections between areas V5 and V1 in macaque monkey visual cortex. Eur J Neurosci 1:310–332.

Spatz WB. 1975. An efferent connection of the solitary cells of Meynert. A study with horseradish peroxidase in the marmoset *Callithrix*. Brain Res 92:450–455.

Tigges J, Tigges M, Anschel S, Cross NA, Ledbetter WD, Mcbride RL. 1981. Areal and laminar distribution of neurons interconnecting the central visual cortical areas 17, 18, 19, and MT in squirrel monkey (*Saimiri*). J Comp Neurol 202:539–560.

Tootell RBH, Hamilton SL, Silverman MS. 1985. Topography of cytochrome oxidase activity in owl monkey cortex. J Neurosci 5:2786–2800.

Ungerleider LG, Desimone R. 1986. Cortical connections of visual area MT in the macaque. J Comp Neurol 248:190–222.

Vogt Weisenhorn DM, Illing R-B, Spatz WB. 1995. Morphology and connections of neurons in area 17 projecting to the extrastriate areas MT and 19DM and to the superior colliculus in the monkey *Callithrix jacchus*. J Comp Neurol 362:233–255.

Winfield DA, Rivera-Dominguez M, Powell TPS. 1981. The number and distribution of Meynert cells in area 17 of the macaque monkey. Proc R Soc Lond B 213:27–40.

Wong-Riley MTT. 1979a. Changes in the visual system of monocularly sutured or enucleated cats demonstrable with cytochrome oxidase histochemistry. Brain Res 171:11–28.

Wong-Riley MTT. 1979b. Columnar cortico-cortical interconnections within the visual system of the squirrel and macaque monkeys. Brain Res 162:201–217.

Wong-Riley MTT. 1989. Cytochrome oxidase: An endogenous metabolic marker for neuronal activity. Trends Neurosci 12:94–101.

Wong-Riley MTT. 1994. Primate visual cortex: dynamic metabolic organization and plasticity revealed by cytochrome oxidase. In: Peters A, Rockland KS, editors. Cerebral cortex. New York: Plenum Press. p 141–200.

Yoshioka T, Levitt JB, Lund JS. 1994. Independence and merger of thalamocortical channels within macaque monkey primary visual cortex: anatomy of interlaminar projections. Visual Neurosci 11:467–490.

Yoshioka T, Blasdel GG, Levitt JB, Lund JS. 1996. Relationship between patterns of intrinsic lateral connectivity, ocular dominance, and cytochrome oxidase-reactive regions in macaque monkey striate cortex. Cerebral Cortex 6:297–310.

Zeki SM. 1974. Functional organization of a visual area in the posterior bank of the superior temporal sulcus of the rhesus monkey. J Physiol 236:549–573.